

Polymer Chemistry

Accepted Manuscript



This is an *Accepted Manuscript*, which has been through the Royal Society of Chemistry peer review process and has been accepted for publication.

Accepted Manuscripts are published online shortly after acceptance, before technical editing, formatting and proof reading. Using this free service, authors can make their results available to the community, in citable form, before we publish the edited article. We will replace this *Accepted Manuscript* with the edited and formatted *Advance Article* as soon as it is available.

You can find more information about *Accepted Manuscripts* in the [Information for Authors](#).

Please note that technical editing may introduce minor changes to the text and/or graphics, which may alter content. The journal's standard [Terms & Conditions](#) and the [Ethical guidelines](#) still apply. In no event shall the Royal Society of Chemistry be held responsible for any errors or omissions in this *Accepted Manuscript* or any consequences arising from the use of any information it contains.



Polymer chemistry

ARTICLE

Effect of Polymer Branching and Average Molar Mass on the Formation, Stabilization and Thermo-responsive properties of Gold Nanohybrids Stabilized by Poly(N-isopropylacrylamide).

Received 00th January 20xx,
Accepted 00th January 20xx

DOI: 10.1039/x0xx00000x

www.rsc.org/

Hong Hanh Nguyen,^a Annie Brûlet,^b Dominique Goudounèche,^c Pascale Saint-Aguet,^d Nancy Lauth-de Viguierie^{*,a} and Jean-Daniel Marty^{*,a}

Branched structures are of crucial importance in the formation of hybrid materials with tunable properties. Nevertheless little is known about the optimal macromolecular parameters (molecular weight, extent of branching...) allowing either to control the growth mechanism of the inorganic core or to have access to nanohybrids with high colloidal stability. In this paper, the synthesis and characterization of a new family of dendritic polymers comprising a branched polyamidoamine core and a poly(N-isopropylacrylamide) shell is described. In aqueous solution, a strong dependency of their thermo-responsiveness upon macromolecular architecture was evidenced by neutron and light scattering techniques and electronic microscopy. These polymers were then employed as stabilizers of gold nanoparticles (Au NPs) dispersions by either a posteriori adsorption on NPs or in situ NPs formation. Both approaches were successful for stabilization and reversibility of the thermostimulable precipitation process. First, we demonstrated that, macromolecular architecture greatly influences the growth mechanism of in situ formed NPs and their colloidal stability. Whereas small linear polymers allow a better control of NPs growth, branched structures proved to be better stabilizing agents. On the contrary, adsorption on preformed AuNPs of controlled size, evidenced the higher efficiency of small branched structures than linear or hyperbranched polymer as for good stabilizing agent.

A. Introduction

In the past decade, particular attention was paid to designing smart synthetic materials capable of responding to small changes in their environment in a controllable and predictable fashion. Environmental stimuli include solvent exchange, temperature, pH, light, magnetic or electric field, ionic factors, chemicals or biological molecules and mechanical stress. These responses are manifested as dramatic changes in the materials properties, dimensions, structure and interactions and may lead to changes in their aggregation state.¹ Hence many polymers have been designed to respond to small changes in their environment. Thermo-responsive polymers correspond to water soluble polymers that upon temperature display changes due to a fine hydrophobic–hydrophilic balance in their structure. Small temperature changes around a critical value induce the collapse

or expansion of polymer chains as a response to the new adjustments of the hydrophobic and hydrophilic interactions between the polymeric chains and the aqueous media. So, this kind of systems exhibits a cloud point temperature (T_c) at which phase separation occurs. When one phase is observed above certain temperature and a phase separation occurs below, the system presents an upper critical solution temperature (UCST). The opposite, one phase below a specific temperature and phase separation above, is a lower critical solution temperature (LCST). Poly(*N*-isopropylacrylamide) (PNIPAM) is by far the most commonly described thermo-responsive polymer but other families such as polyvinylcaprolactame,^{2,3} poly(oligo(ethylene glycol) methacrylate),⁴ poly(methyl vinyl ether)⁵ and poly(*N*-acryloyl-*N*'-propyl piperazine)⁶ have also been used. Incorporation of hydrophilic or hydrophobic comonomers enables to finely tune LCST values.^{7,8} For example, when NIPAM is statistically copolymerized with hydrophilic monomers such as acrylamide, the LCST increases up to about 45 °C when the polymer chain comprises 18 mol% of acrylamide, whereas LCST decreases to about 26 °C when 20 mol% of hydrophobic acrolein is incorporated into the polymer chain.⁷ In a lesser extent, the same trend was observed in the case of block copolymers.⁸ Polymer architecture also influences thermo-responsiveness of those polymers. Hence, PNIPAM chains grafted on four-arm star core are able to collapse to form denser globules than the ones observed for linear PNIPAM.⁹

^a IMRCP, Université de Toulouse, CNRS UMR 5623, 31062 Toulouse Cedex 09, France.

^b Laboratoire Léon Brillouin, UMR12 CEA-CNRS, CEA Saclay, F-91191 GIF/Yvette, France.

^c CMEAB, IFR-BMT, Université de Toulouse, 133 route de Narbonne, 31062 Toulouse, France

^d Technopolym, ICT, FR 2599, Université de Toulouse, 31062 Toulouse, France.

* corresponding authors: JDM : marty@chimie.ups-tlse.fr, NLV : viguerie@chimie.ups-tlse.fr

Electronic Supplementary Information (ESI) available: additional datas concerning the synthesis and characterization of polymers, their thermo-responsive properties in aqueous solutions and the formation of gold nanohybrids.

These thermoresponsive structures have been used as stimuli responsive drug nanocarriers, as nanoreactors or as coating agent to obtain surface with tunable hydrophobicity...^{10,11} In addition, they have also been extensively used to obtain thermoresponsive organic-inorganic hybrid nanocomposites either by a “grafting from” or a “grafting to” approach, or by direct growth of nanoparticles (NPs) within polymer.¹² Indeed, when a thermoresponsive polymer is physically or chemically attached to the surface of NPs, not only a steric stability is acquired, but also the properties of the NPs (catalytic, optical...) can be modified to some extent in response to one of these small changes in temperature.^{2,13,14} In that context, stimuli responsive branched structures have been used to act either as a complexing and growth control agent prior to NPs formation or as stabilizing agent bringing some additional functionalities.¹⁵⁻¹⁷ Indeed, dendritic architectures have shown huge capacity to encapsulate and stabilize metal nanoparticles due to their unique topologies.¹⁸⁻²¹ Hyperbranched polyethyleneglycol grafted with PNIPAM polymer chains have thus been used to stabilize preformed citrate stabilized gold nanoparticles.¹⁵ Upon heating above the cloud point temperature, the surface plasmon band of the coated AuNPs became broader and further red-shifted by 50 nm with a concomitant change in solution colour from clear red to opaque purple. The observed aggregation is completely reversible over multiple cycles, thus revealing the robust nature of this hyperbranched polymer coating. Moreover the transition temperatures of the polymer-encapsulated nanoparticles are slightly lower (3–9 °C) than that of the pure polymer. This resulted from the significant reduction in conformational freedom of the HPG-NIPAM polymers after immobilization at the gold nanoparticle surfaces/core. Hence, the thermoresponsive behavior can significantly differ from the behavior of free chains in solution.²² Liu et al have reported the use of hyperbranched polyethyleneimine functionalized with thermoresponsive isobutyric amide groups (HPEI-IBAm) to stabilize gold NPs.¹⁶ Upon raising the temperature above T_c , a red-shift of the surface plasmon resonance is observed in a narrow temperature range. Interestingly, T_c of the obtained nanohybrid could be easily tuned by modulating the molecular weight or the degree of substitution of the core. Consequently, thermoresponsive AuNPs could act as colorimetric sensors for detecting the variation of temperature, pH or salt concentration.^{16,17} They could also be used as recyclable responsive catalysts for the reduction reaction of 4-nitrophenol by NaBH_4 . As already observed for linear polymer,¹³ the reaction rate was first accelerated by elevating the reaction temperature, but reached a plateau or decelerated upon raising the temperature close to the cloud point temperature of the thermoresponsive AuNPs catalysts.^{16,17} Moreover, reducing the molecular weight of the HPEI core, lowering the degree of substitution values or increasing the concentrations of the capping HPEI-IBAm polymers or the gold resulted in the acceleration of the reaction. Thus, branched structures are of crucial importance in the formation of hybrid materials with tunable properties. Nevertheless little is known about the optimal macromolecular parameters (molecular weight, extent of branching...) allowing

either to control the growth mechanism of the inorganic core or to have access to nanohybrids with high colloidal stability. In this paper, we aim at better understanding the effect of macromolecular architecture on the properties of those nanohybrids. For this purpose, the synthesis and characterization of a new family of dendritic polymers comprising a hyperbranched polyamidoamine core and a PNIPAM dense shell are described. This study has allowed assessing the key macromolecular parameters that control i) the growth mechanism of in situ synthesized gold NPs, ii) the colloidal stability and iii) the thermoresponsive properties of the obtained nanohybrids.

B. Experimental section

B.1. Materials. Tetrachloroauric acid trihydrate ($\text{HAuCl}_4 \cdot 3\text{H}_2\text{O}$), D-Glucosamine hydrochloride, 1,1'-Carbonyldiimidazole, anhydrous DMSO, carboxylic acid terminated PNIPAM 2000, 5000 and 7000 g/mol, Pur-A-Lyzer™ Mega Dialysis Kit of MWCO 3.5 kDa, 6-8 kDa and 12-14 kDa were purchased from Aldrich and were used without further purification. Tris(2-aminoethyl)amine (Aldrich) was distilled under reduced pressure and stored under argon atmosphere before use. Ultrapure water ($\rho=18 \text{ M}\Omega \text{ cm}^{-1}$) was obtained from Aquadem apparatus.

B.2. Polymer synthesis.

The synthesis of the aminoterminated hyperbranched amidoamine H4 and H5 cores were carried out following previously published work.^{23,24}

The synthesis of core-shell polymers were performed using either three-branches molecule TREN (T) or hyperbranched polymer H4 and H5 cores and PNIPAM of different number average molar masses (2000 g/mol, 5000 g/mol and 7000 g/mol noted P2, P5 and P7 respectively). The details of preparation of H4P2 are given below as a typical example (see supporting information for characterization of other compounds). 1g of carboxylic acid terminated P2 ($5.10 \cdot 10^{-4}$ mol, 1 eq.) and 89.2 mg of 1,1'-carbonyldiimidazole ($5.5 \cdot 10^{-4}$ mol, 1.1 eq.) were dissolved in 10 mL dry DMSO. The mixture was stirred overnight under argon at room temperature (25°C). Then, 3.63 mL of a 20 mg/mL H4 in DMSO solution (72.6 mg H4, 0.9 eq. of primary amine) was added slowly in the previous mixture. The reaction was continuously stirred for 24 h under argon at room temperature. Then, the mixture was dialyzed in ultrapure water for 3 days and the final core-shell polymer H4P2 was collected by lyophilization.

TP2: ^1H NMR (D_2O , 300Hz): 1.07 (CO-NH-CH- $\underline{\text{CH}_3}$, PNIPAM), 1.51 (CH- $\underline{\text{CH}_2}$, PNIPAM), 1.94 ($\underline{\text{CH}}-\text{CH}_2$, main chain PNIPAM), 2.36 (N- $\text{CH}_2-\underline{\text{CH}_2}$ -NH-CO), 2.45 (N- $\underline{\text{CH}_2}$ - CH_2 -NH-CO), 2.60 (CO- $\underline{\text{CH}_2}$ - CH_2 -S, PNIPAM), 2.70 (CO- $\text{CH}_2-\underline{\text{CH}_2}$ -S, PNIPAM), 3.83 (CO-NH- $\underline{\text{CH}}$ - CH_3 , PNIPAM)
IR (TP2) : $\bar{\nu} = 3434, 3289, 3075, 2971, 2932, 2875, 1642, 1543, 1458, 1386, 1366, 1263, 1172, 1130, 1025, 927, 881, 838 \text{ cm}^{-1}$

H4P2: NMR, 300MHz, D₂O, ¹H: 1.0. (CO-NH-CH-CH₃), 1.44 (CH-CH₂), 1.87 (CH-CH₂ main chain PNIPAM), 2.28 (CO-CH₂-CH₂-S), 2.37 (N-CH₂-CH₂-CO), 2.45 (N-CH₂-CH₂-N), 2.53 (CO-NH-CH₂-CH₂), 2.55 (CO-CH₂-CH₂-S), 2.63 (N-CH₂-CH₂-CO), 3.23 (CO-NH-CH₂-CH₂), 3.75 (CO-NH-CH-CH₃); ¹³C: 21.7. (CO-NH-CH-CH₃), 27.80 (CO-CH₂-CH₂-S), 35.01 (CH-CH₂), 35.09 (N-CH₂-CH₂-CO), 36.51 (CO-NH-CH₂-CH₂), 37.05 (CO-CH₂-CH₂-S), 41.8 (CO-NH-CH-CH₃), 42.7 (CH-CH₂ main chain PNIPAM), 51.1 (N-CH₂-CH₂-CO), 52.0 (CO-NH-CH₂-CH₂), 53.6 (N-CH₂-CH₂-N), 174 (CO-NH). IR (H4P2): $\bar{\nu}$ = 3434, 3288, 3073, 2972, 2933, 2857, 1641, 1542, 1458, 1386, 1366, 1268, 1172, 1130, 1026, 975, 927, 882, 838 cm⁻¹.

In all cases, PNIPAM was added with a slight excess relatively to the number of primary amine available. Therefore only hyperbranched structures with a dense PNIPAM shell were obtained. Measured molar grafting ratio were found from FTIR and DSC measurements around 70% depending on both hyperbranched core size and PNIPAM chain length (see Table 1).

B.3. Nanoparticles synthesis.

Ex situ synthesis of AuNPs. 35 μ L of freshly prepared NaOH (1 mol·L⁻¹) solution were added to 18.86 mL of ultrapure water under magnetic stirring. Then 1 mL of HAuCl₄ 0.01 mol·L⁻¹ solution was added, the solution became pale yellow. Finally 100 μ L of freshly prepared NaBH₄ 0.1 mol·L⁻¹ were added under vigorous stirring. The solution changed from pale yellow to deep red immediately. The solution was stable for several weeks. [NaOH]/[NaBH₄]/[HAuCl₄]=3.5/1/1.

AuNPs were then stabilized with the chosen polymer at different concentration (from 5.10⁻² wt.% to 10⁻⁶ wt %). The final [Au] was fixed at 2.5 10⁻⁴ mol·L⁻¹. The protocol for stabilization with final polymer concentration of 10⁻² wt% was the following: 10 μ L of 0.2 wt.% polymer stock solution were added to 90 μ L of water, then 100 μ L of 5.10⁻⁴ mol·L⁻¹ gold colloid solution were added.

In situ synthesis of AuNPs. 10 μ L of 0.1 wt % polymer stock solution were added to 85 μ L of water, then 100 μ L of 5.10⁻⁴ mol·L⁻¹ gold colloid solution were added. Then 5 μ L of freshly prepared 0.01 mol·L⁻¹ NaBH₄ solution was added under shaking, corresponding to a molar ratio [NaBH₄]/[HAuCl₄]=1/1. Finally, the solution became red.

B.4. Apparatus.

Size Exclusion Chromatography (SEC). Average number molecular weights (M_n) and polydispersity indexes (\bar{D}) were determined by SEC on an apparatus equipped with a Waters 2140 refractive index (RI) detector, using a Waters Styragel HR 4E column (40°C, eluent, THF, flow rate, 1 mL·min⁻¹). Typically, samples at a concentration of 5 mg·mL⁻¹ in THF were injected. Alternatively, samples were analyzed with a SEC apparatus comprising a Varian ProStar 325 UV detector (dual wavelength analysis) and a Waters 410 refractive index detector, using two Shodex K-805 L columns (8 mm, 300 mm, 13 μ m) and DMF LiCl (1 g·L⁻¹) as the eluent at 40°C (flow rate, 1 mL·min⁻¹).

Nuclear Magnetic Resonance. To determine the structural characteristics of the polymers, NMR experiments were performed at 298K in D₂O on a Bruker AVANCE 300 MHz or 500 MHz spectrometer equipped with a 5 mm Z-gradient TCI cryogenic probe. The 90° pulse length was 9 μ s, the sweep width was 10 kHz and the acquisition time was 3.5 s. The scan number was adjusted to obtain a sufficient signal to noise ratio and the relaxation delay between transients was 3s. For 1D 1H experiments, a 30° pulse was used. Attribution of the signals was made by COSY, HSQC and HMBC experiments.

Fourier Transform Infra Red (FTIR). Spectra were recorded with a Nexus Thermo Nicolet spectrometer equipped with a detector DTGS, in attenuated total reflection (ATR) mode with a diamond crystal in the spectral region of 600-4000 cm⁻¹ with a resolution of 2 cm⁻¹. The physical mixtures were prepared by simple homogenization of HYPAM and PNIPAM as followed: 2 mL of an aqueous solution of HYPAM (5 mg·mL⁻¹) was prepared. To this solution was added 5 mL, 4.5 mL, 3.75 mL, 2.5 mL of (25 mg·mL⁻¹) aqueous PNIPAM affording the 1 : 1, 1 : 0.90, 1 : 0.75 and 1 : 0.5 ratios respectively. The obtained solution was then freeze-dried and the spectra of the obtained solids were recorded.

Differential Scanning Calorimetry (DSC). The thermal properties of the polymer (in solution and in bulk) were determined by DSC using a Mettler Toledo DSC 1 STARE System Thermal Analysis calorimeter equipped with a Gas Controller GC200. Solid samples were sealed inside aluminum crucibles of 40 μ L, glass transition temperatures were taken at inflection points as the temperature increased at different rates: 30, 20, 10°C·min⁻¹. Solution samples were sealed in impermeable crucibles of 120 μ L. Transition temperatures were taken at the top of the DSC peaks as the temperature increased at different rates; 10, 5, 2 and 1 °C·min⁻¹, and finally extrapolated to 0 °C·min⁻¹. The variation of enthalpy was measured as the temperature increased at a rate of 10 °C·min⁻¹.

Small Angle Neutron Scattering (SANS). SANS experiments were performed with the PACE spectrometer at the Orphée reactor (LLB, Saclay). Polymer solutions in D₂O solvent were put inside quartz cells of 2 mm path length. ([polymer] = 1 wt %). Two spectrometer configurations were used: a neutron wavelength (λ) of 6 Å with a sample to detector distance of 3 m and a wavelength of 13 Å with a distance of 4.7 m. The scattering vector range thus reached was 0.0032 < q (Å⁻¹) < 0.12. Scattering intensities were normalized by the incoherent signal delivered by a 1 mm gap water sample in order to account for the efficiency of the detector. Absolute values of the scattering intensity, I(q) in cm⁻¹, were obtained from the direct determination of the number of neutrons in the incident beam and the detector cell solid angle. No background was subtracted to the sample scattering, thus a flat incoherent signal was observed at high q values. Data treatment was done with the Laboratoire Léon Brillouin software.

Dynamic Light Scattering (DLS). DLS was carried out on a Malvern Zetasizer NanoZS equipped with a He-Ne laser (λ =633 nm). The correlation function was then analyzed via the general-purpose non-negative least squares (NNLS) method to obtain the intensity-weighted distribution of diffusion

coefficients (D) of the solutes. This distribution can be converted, using Mie theory, to a number-weighted distribution describing the relative proportion of multiple components in the sample based on their number rather than based on their scattering. The average apparent hydrodynamic diameter, noted as D_h were determined using the Stokes-Einstein equation from number-weighted distribution respectively. The typical accuracy for these measurements was 10-15%. It has to be mentioned that the determination of D_h assumed non interacting particles modeled with a homogeneous spherical hard sphere models.

Turbidity measurements. Transmittance of polymer aqueous solutions was recorded with a HP 8452A diode array spectrophotometer with increasing temperature at different heating rates at a wavelength of 500 nm. The cloud points were then calculated by the extrapolation to $0\text{ }^\circ\text{C min}^{-1}$ of the cloud points obtained from the inflection point of each transmittance curve.

Transmission electron microscopy (TEM). A drop of the aqueous dispersion was placed on a formvar carbon-coated copper TEM grid (Ted Pella Inc.) and left to dry under air. For samples needing negative staining, the TEM grid was successively placed on a drop of the sample solution for 1 min and on a drop of an aqueous solution of uranyl acetate (2 wt %, 10 s), after which the grid was then air dried before introduction into the electron microscope. To visualize mesoglobules, we heated polymer solutions (45°C) for 1 h prior to the deposit. The previously described procedure for preparation of TEM grids was then employed; however, they were dried in an oven at 45°C . The samples were viewed with a MET Hitachi HT7700 transmission electron microscope operating at 80 kV accelerating voltage. Size-distribution histograms were determined by using magnified TEM images. The size distribution of the particles was determined by measuring a

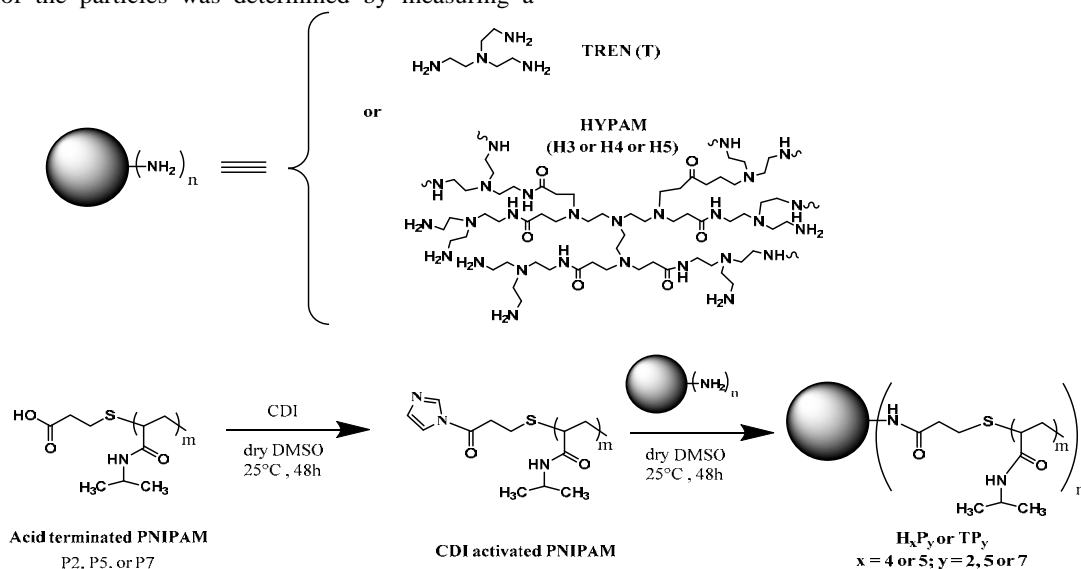
minimum of 200 particles of each sample, using WCIF Image J software. The size distributions observed were analyzed in terms of Gaussian statistics ($wc(\sigma)$).

C. Results and discussion

C.1. Synthesis and characterization of the hyperbranched polymers consisting of the PNIPAM shell and hyperbranched polyamidoamine core.

The synthesis of three-branched or hyperbranched polymers are outlined in Scheme 1. The core of the three branched polymers was a trisamine molecule (tris(2-aminoethyl)amine, TREN noted T). Amino-terminated hyperbranched polyamidoamine cores (HYPAM) with a structure similar to the one of PAMAM dendrimers²⁵ were synthesized following a previously published procedure.²⁶ In this procedure, tris(2-aminoethyl)amine was reacted with a hexaester (tris(2-di(methylacrylate)aminoethyl)amine) leading in a single step to hyperbranched cores.

Molecular weight of these hyperbranched polymers was easily adjusted by changing the ratio between the reactants. TREN on hexaester molar ratios close to 12:1, 10:1 or 8:1 led to polymers with molecular weight close to those of PAMAM of the third, fourth and fifth generation and were noted H_3 or H_4 or H_5 respectively. From size exclusion chromatography, the mass average molar masses of the three cores were evaluated at 5200, 13000 and 27000 $\text{g}\cdot\text{mol}^{-1}$ respectively and the number of primary amine groups obtained from quantitative ^{13}C NMR were 5.0, 6.2 and 4.2 $\text{mmol}\cdot\text{g}^{-1}$ respectively.



Scheme 1. Synthesis of HYPAM-based branched or hyperbranched polymers with a core-shell structure.

Polymer Chemistry Accepted Manuscript

Moreover, small-angle neutron scattering (SANS) measurements were carried out to quantitatively analyze the size and conformation of the H3, H4 and H5 cores in D₂O solution at 20°C. Figure 1 shows the scattering vector q dependence of the measured neutron scattering intensity $I(q)$ of H3, H4 and H5 solutions in D₂O (1 wt %).

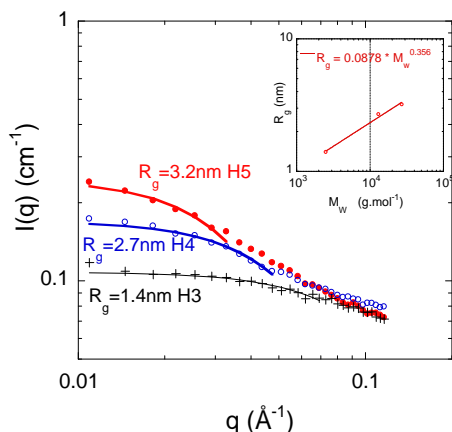


Figure 1. SANS curves for the hyperbranched hypam H3, H4 and H5 in D₂O (1 wt %). Lines are best fits to the Guinier law allowing to deduce the radius of gyration R_g of polymers. In the inset, the double-logarithmic plot of R_g versus the weight average molecular weight (determined by SEC) of hyperbranched polymers with the best fit to a power law with an exponent 0.356.

The scattering intensity reached a plateau at low q which demonstrates that entities with defined molar mass are present. These traces can be fit using the Guinier model which provides an estimate of the gyration radius (R_g) of these hyperbranched polymers. As expected, the R_g values increase with the polymer generation: 1.4, 2.7, and 3.2 nm for H3, H4 and H5 respectively. Further structural information is obtained from the dependence of the radius of gyration on the weight average molecular mass (Figure 1, inset). The double-logarithmic plot of R_g vs M_w shows a linear dependence (Figure 1 inset), with a power law, $R_g = 0.0878 M_w^{0.356}$. The slope of this linear plot is 0.356 and thus is very close to 1/3, which is found for spheres. This indicates H3, H4 and H5 hyperbranched polymers are collapsed in compact spherical objects, as already observed in others hyperbranched polymers.²⁷ The sizes are similar of those found for PAMAM from light scattering measurements: respectively 1.5 nm, 2.0 nm and 2.6 nm for generation 3, 4 and 5.²⁸ This proved the unimolecular feature of hyperbranched polymers.

Poly(*N*-isopropyl acrylamide) (PNIPAM) with three different number average molar masses M_n of 2000, 5000 or 7000 $\text{g}\cdot\text{mol}^{-1}$ (P2, P5, P7) were grafted to the amino-terminated cores (T, H4, H5) chains by an amide coupling reaction as shown in Scheme 1. First, carboxylic acid terminated PNIPAM is reacted with 1,1'-carbonylimidazole (CDI) in dried DMSO to form carbonylimidazolide-terminated PNIPAMs. Then activated PNIPAMs were added onto the amino-terminated HYPAM cores to form the core-shell architectures. The

obtained compounds, noted TP2, 5 or 7 and HxP2, 5 or 7 with $x = 4$ or 5, were purified by dialysis. Their main characteristics were summarized in Table 1.

Table 1. Macromolecular characterization of hyperbranched structures determined from ATR-FTIR and DSC measurements

Sample	Macromolecular characteristics				Grafting ratio		Behavior in solution	
	M_{theo}^a (g/mol)	pnipam theo wt %	Number of pnipam chains theo	T_g (°C)	FTIR	DSC	T_c (°C)	ΔH (J/g)
P2	2000	100%	/	112.3	/	/	32.1	20.5
P5	5000	100%	/	130.1	/	/	32.7	19.0
P7	7000	100%	/	133.3	/	/	33.4	18.5
TP2	5300	97%	2.6	119.1	86%	87%	33.9	20.0
TP5	13000	99%	2.6	130.7	87%	89%	34.1	18.8
TP7	17000	99%	2.4	136.4	81%	83%	33.0	18.4
H4P2	56000	88%	24.7	122.6	61%	49%	33.3	18.5
H4P5	135000	95%	25.7	130.2	64%	72%	34.0	18.2
H4P7	192000	97%	26.5	135.0	66%	71%	33.4	17.9
H5P2	73000	84%	30.6	85.8	62%	51%	33.8	18.0
H5P5	182000	94%	34.1	127.6	69%	73%	34.4	17.9
H5P7	253000	95%	34.5	138.7	70%	79%	33.6	17.8

^a $M_{\text{(theoretical)}}$ was calculated using the grafting ratio from FTIR method

The successful grafting of P2 onto branched core was first evidenced by size exclusion chromatography in DMF as eluant with 1 $\text{g}\cdot\text{L}^{-1}$ LiCl. Figure 2 and Figure SI1 in ESI showed SEC traces for P2, TP2, H4P2 and H5P2. Grafting of P2 to the hyperbranched core (TREN or HYPAM) led as expected to a shortened elution time.

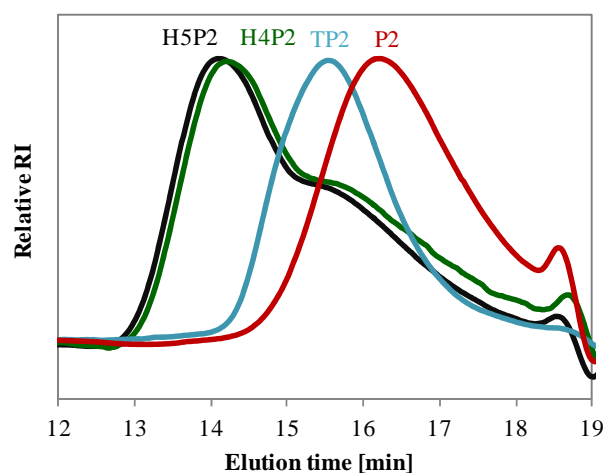


Figure 2. Superposition of normalized SEC chromatograms (RI detection in DMF with 1 $\text{g}\cdot\text{L}^{-1}$ LiCl) of P2, TP2, H4P2 and H5P2.

Whereas the first two polymers present a rather thin width of peaks, hyperbranched based polymers present larger elution profile, as expected from the large dispersity of the pristine HYPAM polymers used as a core. The experimental mass average molecular weight values and corresponding dispersity were found equal to 2800 ($\mathcal{D} = 1.2$), 5600 ($\mathcal{D} = 1.3$), 30600 ($\mathcal{D} = 1.9$) and 31200 $\text{g}\cdot\text{mol}^{-1}$ ($\mathcal{D} = 2.0$) for P2, TP2, H4P2 and H5P2 respectively. Discrepancies with theoretical values (Table 1) arise from the intrinsic nature of those polymers with a hyperbranched core-shell architecture. Therefore, a regular analysis with standard calibration is not valid. The use of light scattering detector together with a refractometric one provides an evaluation of the molecular weight of the polymers. However, even with this approach, for wide distributions, the difference of sensitivity of light scattering between high and low molecular masses leads to an underestimated polydispersity index.⁷ Furthermore, these polymers (as well as PAMAM dendrimers) have been observed to trap solvent molecules even after prolonged drying. Thus, the measured molecular weights should be considered only as indicative values. Therefore in Table 1 are also given theoretical molecular weights estimated from the measured average molecular weights in number of hyperbranched cores²⁶ and from the degree of functionalization estimated from FTIR experiments.

The amide coupling between TREN or HYPAM cores and the carboxylic acid terminated Poly(*N*-isopropyl acrylamide) was further evidenced by ATR-FTIR and ¹H NMR experiments on dialyzed samples as illustrated in Figure S12 in ESI and Figure 3 (see also Figure S13 in ESI).

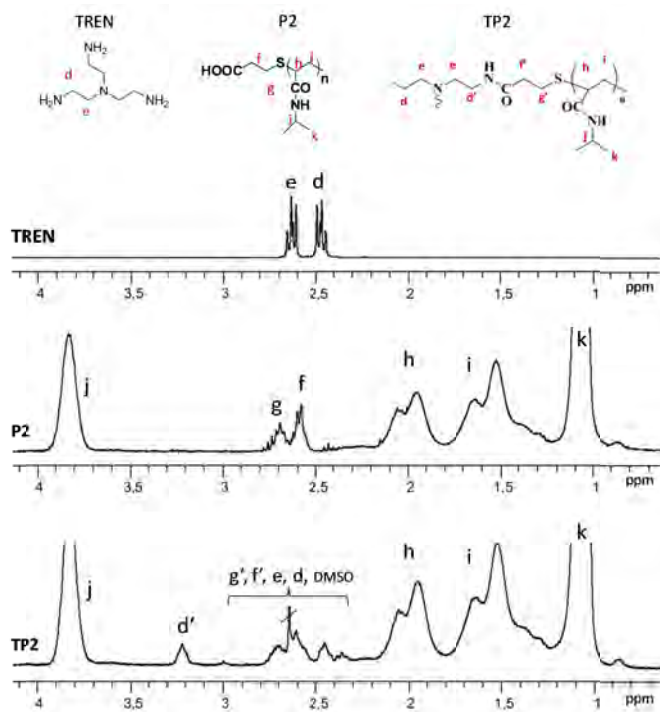


Figure 3. ¹H-NMR spectra for TREN, P2 and TP2 in D₂O.

In ATR-FTIR the disappearance of C=O stretching band of carboxylic function at 1712 cm^{-1} corresponding to carboxylic acid terminated poly(*N*-isopropylacrylamide) was accompanied with the appearance of a new absorbance band at 2934 cm^{-1} characteristic of methyl moieties (Figure S12 in ESI). Moreover, an additional peak at 3.23 ppm assigned to proton in α position of the forming amide groups (noted d') was clearly identified on ¹H NMR of TREN-PNIPAM (Figure 3). In the case of hyperbranched cores, the proton in α position of the forming amide groups coincide with the one already exists in the structure of the core (Figure S13 in ESI). Moreover, PGSE NMR spectroscopy (Figure S14 in ESI) allows to determine a self-diffusion coefficient, *D*, for grafted polymer lower than for the corresponding PNIPAM homopolymer: thus in the case of H4P5 $D = 0.4 \cdot 10^{-10} \text{ m}^2 \cdot \text{s}^{-1}$ whereas it is twice lower in the case of P5 ($D = 0.8 \cdot 10^{-10} \text{ m}^2 \cdot \text{s}^{-1}$).

The degree of grafting of hyperbranched cores by the PNIPAM homopolymers was calculated using ATR-FTIR spectroscopy and confirmed by DSC analysis. This degree was determined relatively to the number of terminal NH₂ groups. By FTIR (Figure S12 in ESI), this molar ratio is proportional to the ratio of the intensity of the C-H deformation bands of methyl groups ($\nu = 1386 \text{ cm}^{-1}$) to the intensity of carbonyl stretching bands of amide function ($\nu = 1642 \text{ cm}^{-1}$). Calibration curve was obtained by measuring this ratio on spectra of the physical mixtures of H4 and P7 (Figure S15 in ESI). This degree was also evaluated from DSC experiments of 0.5 wt.% polymer solution. For this, the variation of enthalpy registered for a given polymer was compared to the variation measured for pure PNIPAM at the same concentration, assuming that grafting does not modify significantly the energy involved during the dehydration process (Figure S18 in ESI, calculation see Part A.2.2 in SI). All the results are summarized in Table 1. Both degree of polymerization estimated by those two techniques were in good agreement, around 70 % which is a usual value found for this kind of materials.²⁹

Differential scanning calorimetry (DSC) analyses were performed on all crude polymers (see Figure S16 in ESI). A glass transition temperature (*T_g*) was evidenced for all polymers as reported in Table 1. The latter arises from PNIPAM polymer. As expected shorter PNIPAM chains led to a significant decrease of *T_g* value whatever the core of the polymer. Along with this first transition temperature, a second one, barely visible around -20°C, arises from HYPAM core (see Figure S17 in ESI).

C.2. Properties of aqueous solutions of hyperbranched polymers.

All polymers were dissolved in aqueous solutions with a weight mass fraction between 0.1 and 1%. SANS and electronic microscopy were then used to understand the colloidal structure of the branched structure below and above transition temperature.

First the structure of those polymers was assessed below cloud point temperature. Figure 4 showed that the scattering intensity of the hyperbranched core-shell structures was much larger than the ones of the core and no plateau was observed

at low q . These results indicated the presence of large fluctuations in the solutions.

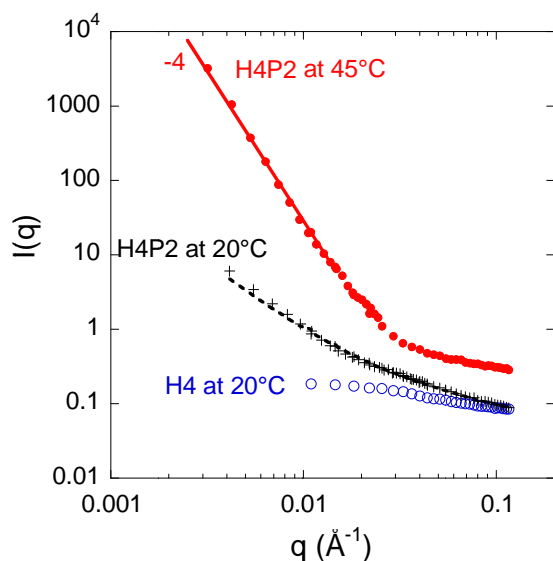


Figure 4. SANS of H4 and H4P2 at 20°C and 45°C. Dotted lines on the curve at 20°C is the best fit to a fractal aggregate model. [Polymer] = 1 wt %.

These differences could not be solely explained by the presence of a PNIPAM corona but suggest that an aggregation phenomenon occurs between hyperbranched polymer chains. This aggregation process between individual dendritic multishell architectures had been previously described for hyperbranched core-shell structures by R. Haag and coll.³⁰ Characteristic size of the subdomain existing in the aggregates could be deduced from fluctuations observed at large distances (low q upturn). These fluctuations that have been characterized by a simple correlation length ξ deduced from fits at large q . These correlation lengths, listed in Table 2, are normally increasing with the molecular weight of PNIPAM branches.

Table 2. Correlation length deduced from fit of SANS curves obtained at 20°C on PNIPAM-based hyperbranched structures.

	ξ (nm)		
	P2	P5	P7
H4	3	3.7	3.9
H5	3.1	3.7	4.3

Direct observations of these supramolecular aggregates were performed by CryoTEM measurements. The CryoTEM micrographs of H4P7 solution confirmed the presence of large aggregates with diameter around 108 ± 23 nm (inset in Figure 5 and Figure S19B in ESI). This size is in good agreement with previous report on aggregation of hyperbranched core-shell structures.³⁰ Stained TEM images of dried aqueous solutions show also regular monodisperse spherical nanoobjects with large diameters (Figure 5 for H4P7, see Figures S19-11 in ESI for others polymers). Interestingly, the micrographs reveal a noticeable granular fine structure and a high contrast for the larger aggregates. The ultrastructural features are fundamentally different from the TEM images of liposomes

and micelles, thus suggesting that the aggregates are indeed formed by a large number of “elementary” unimolecular units. All these results tend to demonstrate the aggregation in aqueous solutions for concentration above 0.1 wt %. Indeed, increasing concentration of polymer up to 20 wt %, nanogels structures were formed through hydrogen bonds between amide functions.³¹

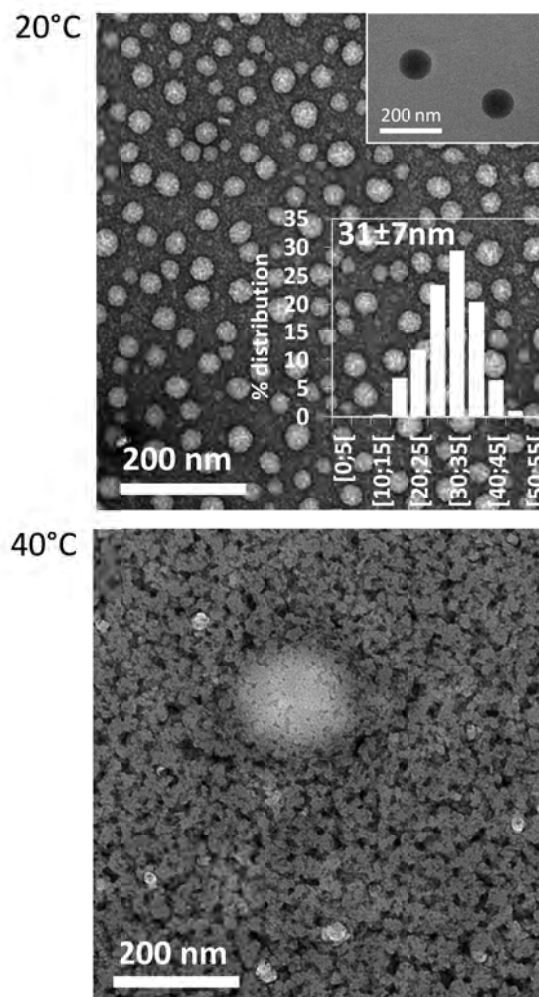


Figure 5. Representative TEM images of H4P7 0.1 wt.% solution samples stained with uranyl acetate at 20°C and 40°C. Inset: Cryo-TEM image of polymer H4P7 at 0.5 wt % in water at 20°C. At 40°C, H4P7 is present as large aggregates with no defined structures.

When solutions of those hyperbranched structures were heated, a transition temperature occurred that corresponds to the transition between the hydrated and dehydrated form of PNIPAM polymer. This phenomenon is clearly evidenced by turbidimetry measurements and DLS measurements as depicted in Figure 6. A hysteresis between the heating process and the cooling process could be observed for all solutions, which was accentuated for higher heating/cooling rates (see supporting information Figure S12 in ESI). This phenomenon can be explained by the fact that the swelling of the compact aggregates formed at higher temperatures is relatively difficult because of intrachain entanglements.

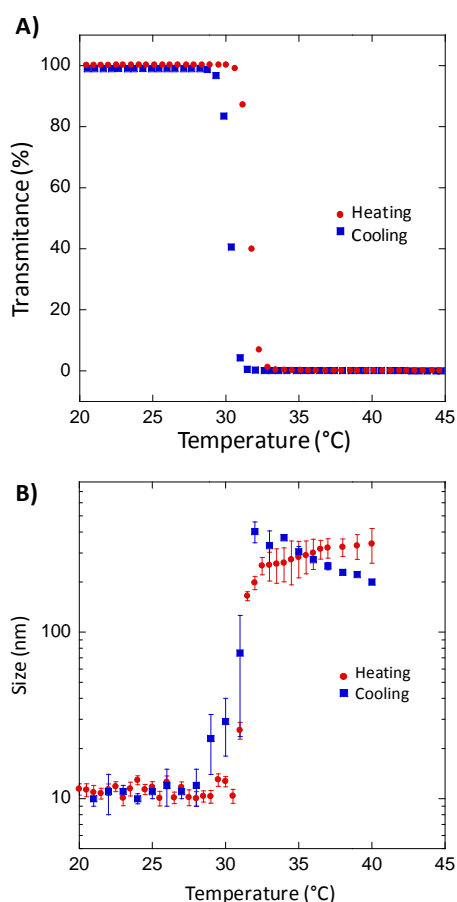


Figure 6. Evolution of (A) transmittance monitored at 500 nm on heating and cooling ($1^{\circ}\text{C}/\text{min}$) and (B) hydrodynamic diameter (D_h) obtained from DLS measurements for a 0.1 wt% solution of H5P7 in water between 20 and 45°C .

Cloud point temperatures (T_c) were determined by DSC experiments by extrapolating values at the peak maximum to $0^{\circ}\text{C}\cdot\text{min}^{-1}$. The values are reported in Table 1 as well as the corresponding associated variation of enthalpy. Cloud point temperatures were all found around $33.0 \pm 1^{\circ}\text{C}$ which is close to cloud point values of free PNIPAM. Therefore grafting of PNIPAM to the HYPAM does not significantly modified characteristics temperatures observed. Above T_c , diffusion experiments evidenced the formation of very large aggregates with a hydrodynamic diameter above 300 nm (Figure 6B). As shown on Figure 5, those aggregates seem to have no defined morphology or size when observed with TEM (for other polymers see also Figures S19-11 in ESI). Huge increasing of the SANS intensities above the cloud point of PNIPAM observed for all samples (see Figure 4 for H4P2) confirmed the formation of large aggregates. Moreover, the characteristic Porod's law (slope -4) observed at low q is indicating the formation of aggregates with sharp interfaces with the solvent. The effect of both PNIPAM chain length and core size is more critical when considering the hydration/dehydration process. This effect was evaluated for each polymer from the transmission profile by evaluating the variation of temperature (ΔT) needed to decrease 100% down to 10% of transmitted signal once the transition occurred (see Figure 6A). All results were reported in Figure 7 (see also Figures S112-S113 in ESI).

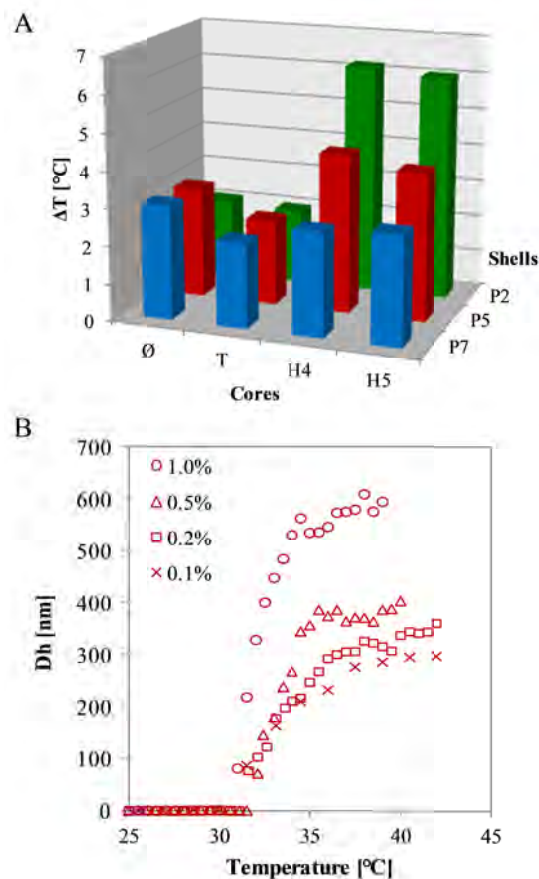


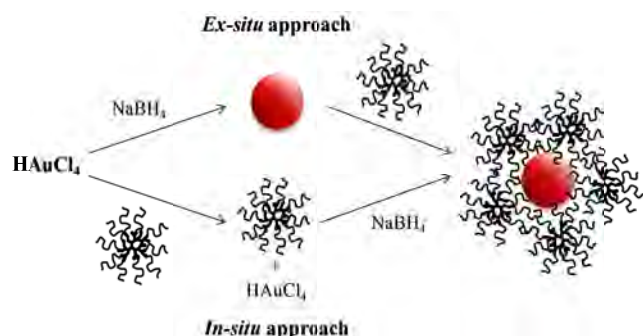
Figure 7. A) Variation of temperature needed to reach 10% of transmission when considering the variation of transmission measured by UV spectroscopy at 500 nm ([polymer]=0.1 wt % in water, heating rate = $1^{\circ}\text{C}\cdot\text{min}^{-1}$). B) Variation of D_h at different concentrations of H4P2 polymer in water (blue: 0.1 wt%, red: 0.2 wt %, green: 0.5 wt %, black: 1.0 wt %).

Whereas the grafting of PNIPAM onto TREN does not modify significantly ΔT comparatively to PNIPAM, its grafting on HYPAM core induced a slower process: ΔT is thus increased from 2°C for P2 and TP2 to 7°C for HxP2. Moreover decreasing PNIPAM chain length from 7000 up to 2000 g/mol, led to a significant increase of ΔT (from 7°C to 2°C for H5P2 and H5P7 respectively). This observation could not be ascribed to the kinetics of PNIPAM dehydration that occurs in very short timescale (typically few seconds). This is more related to the weight fraction of HYPAM hydrophilic core. Indeed decreasing PNIPAM chain length from 7000 up to 2000 $\text{g}\cdot\text{mol}^{-1}$ tend to increase the weight fraction of hydrophilic core (see Table 1). Thus, when increasing temperature above T_c , polymer with high content of PNIPAM chains (i.e. low weight fraction of HYPAM core) quickly dehydrated to form very large aggregates that efficiently scattered the light. For higher hydrophilic fraction (as in the case of H4P2 and H5P2) a different behavior was observed by DLS experiments (Figure 7B): upon T_c , hyperbranched structures are still partially hydrated and formed aggregates with limited size around 100 nm. This size then increased slowly up to few hundred nm when increasing temperature from T_c to 36°C , after which the average size remained constant in solution. This corresponds to a gradual

dehydration process of PNIPAM polymer chains that might be slowed down by the presence of the hydrated attached HYPAM structures. Therefore, the variation observed for transmission signal reflected this slow modification of the average size of the scattering objects and led to an apparent increase of ΔT values. This trend was confirmed when hydrodynamic diameter is registered as a function of temperature for different concentrations. As expected more concentrated solutions tend to favor the aggregation process in aqueous solutions and therefore tend to decrease ΔT values for a chosen polymer.

C.3. PNIPAM based hyperbranched structures as stabilizing agent of preformed gold NPs.

Two different strategies of synthesis of gold nanohybrids have been followed (Scheme 2). For the *ex situ* strategy, AuNPs were synthesized separately and subsequently mixed with the polymer by using a grafting from approach. Through this, a direct comparison of the stabilization and thermoresponsive properties of different families of polymer is made possible. In addition, this also prevents any chemical modification of the polymers that could occur during NPs formation. Besides, in order to evaluate the effect of macromolecular parameters on the growth of gold NPs, an *in situ* strategy has also been used. It will be described in a second time.



Scheme 2. Stabilization of gold nanoparticles in presence of thermoresponsive polymers by either an *in situ* or *ex situ* strategy.

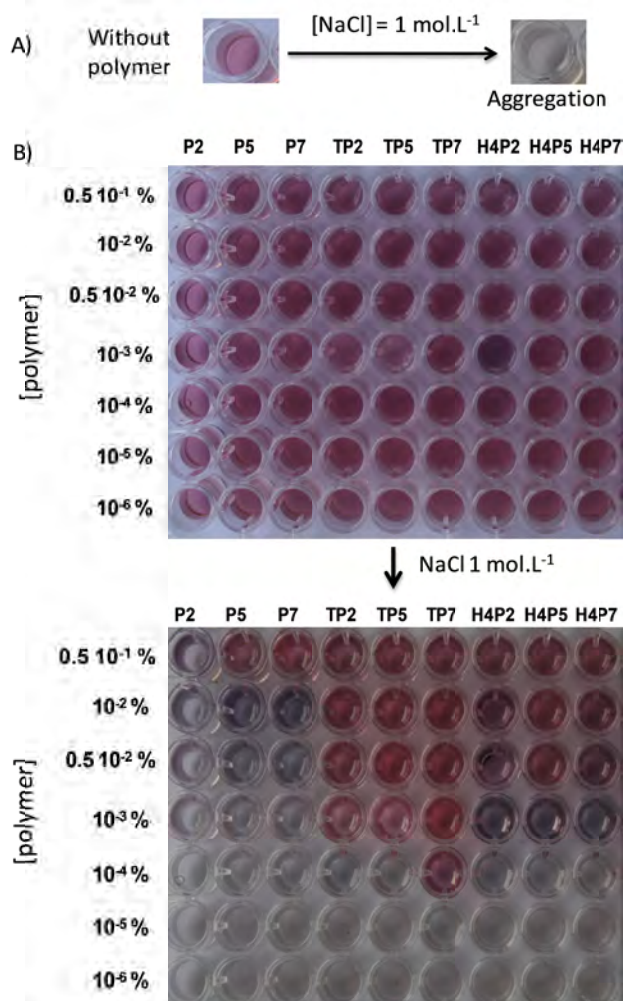
For the first *ex situ* method, preformed AuNPs synthesized by a method allowing the use of small amount of stabilizing agent is preferred. Indeed, getting rid of these stabilizing agents will require tedious step of purification after ligand exchange with the hyperbranched structures to obtain purified nanohybrids. For this, a synthetic protocol using a direct reduction of HAuCl_4 by NaBH_4 was selected.³² Whereas no additional stabilizing agent was added, experimental conditions such as pH and gold precursor concentration have to be carefully chosen to obtain well-controlled AuNPs with good stabilization properties. First, the pH value of the HAuCl_4 needs to be adjusted around 8.0 before addition of NaBH_4 solution: in such conditions, HAuCl_4 was present mainly as $\text{Au}(\text{OH})_4^-$ whose reduction favored the formation of AuNPs as single colloids. In addition, gold concentration need to be kept below $5 \times 10^{-4} \text{ mol} \cdot \text{L}^{-1}$ to avoid further aggregation of AuNPs (Figure SI14 in

ESI). The NPs dispersions thus obtained exhibited a broad absorption band around 516 nm, resulting in a pink-red color of the dispersions. TEM measurements showed isolated AuNPs with an average diameter of approximately $5 \pm 2 \text{ nm}$ (Figure SI15 in ESI). In addition, their hydrodynamic radius measured by DLS was found at $7.3 \pm 0.7 \text{ nm}$, confirming the presence of mainly single colloid in the solutions. NPs are negatively charged (due to the presence of chloride, hydroxide and borate derivatives ions at the surface of the NPs) with a zeta potential around $-30 \pm 2 \text{ mV}$. They are also stable in pure water with no significant change of optical properties over one month period (Figure SI15 in ESI). Any increase of the ionic strength or change in pH is inducing charge neutralization and then aggregation. Thus, increasing ionic strength of the AuNPs dispersion modified the color of the solution from red to purple. This corresponded to a large change of the UV-visible spectrum of the solution: the surface plasmon band (SPB) of the NPs initially at 520 nm (associated to well-dispersed AuNPs) decreased strongly and was accompanied by an increase in absorbance at higher wavelength (suggesting aggregated AuNPs).

The effect of the polymer concentration and the macromolecular architecture on the stability of the hybrids was subsequently studied by monitoring the surface plasmon band (see Figures SI16-18 in ESI). For this, an adequate amount of polymer solution was added to AuNPs solutions to reach the final polymer concentration (from 1×10^{-6} to $5 \times 10^{-2} \text{ wt.}\%$). When the polymer was introduced in the medium, the plasmon band shifted from 518 nm for bare particles to 522 nm up to 527 nm depending on the polymer nature and on the polymer concentration. This bathochromic shift of the maximum wavelength is consistent with the change of the dielectric constant around the particles and demonstrates the efficiency of polymers to interact with the surface of AuNPs. This shift is only observed for polymer concentration above $10^{-4} \text{ wt.}\%$.

The polymer/gold hybrids resulting from the addition of the different polymers were stable over several weeks. Conversely, the solution of bare AuNPs is stable only for a few days. The role of the polymer is of course predominant for NPs stability and we then decided to challenge it against the addition of sodium chloride salt which is known to induce gold NPs aggregation (see Figure 8). Two different mechanisms are assumed to append when salts are introduced in the medium. In the case of bare AuNPs, the surface charges are screened thus promoting their immediate aggregation. For polymer-coated-particles, a salting-out effect takes place, increasing the hydrophobic interactions between the polymer chains, which also leads to aggregation.

Figure 8. Stabilization of preformed Au NPs without polymers (A) or with HxPy



polymer aqueous solution (B) at different concentrations (from $1 \cdot 10^{-6}$ to $5 \cdot 10^{-1}$ wt.%) before and after addition of NaCl (final concentration of NaCl is $1 \text{ mol} \cdot \text{L}^{-1}$, $[\text{Au}]_0$ is fixed at $2.5 \cdot 10^{-4} \text{ mol} \cdot \text{L}^{-1}$).

In the present experiments, when poorly stabilized particles were in presence of $\text{NaCl } 1 \text{ mol} \cdot \text{L}^{-1}$, the solution turned immediately blue with a SPB shift up to 565 nm for bare NPs. With this approach, we clearly got access to the minimal polymer concentration needed to efficiently stabilize the hybrids. As evidence on the 96-well plates experiments, depending on the nature of the polymer, this minimum varies between 10^{-4} to 0.5×10^{-1} wt %. Linear PNIPAM structures were found to be the less efficient to stabilize NPs: only P5 and P7 at 0.05 wt.% were able to successfully stabilize AuNPs. Linear PNIPAM polymers terminated by a carboxylate moiety conferred to the NPs a lower stability in comparison with thiol or thioester end groups. These results are consistent with previous results. It was found that PNIPAM needed to be end terminated by suitable anchoring group (like thiol or thioester)

to be able to interact properly with the surface of AuNPs and to strengthen non specific interaction of PNIPAM moieties with NPs surface.³³ Other branched structures require only concentration down to 10^{-4} wt.% to avoid any aggregation process. Among them, TREN based structures (TP2, TP5 and TP7) proved to be the most effective. Indeed, for HYPAM based structures an aggregation phenomenon is still observed for concentration up to 0.5×10^{-2} wt.%. Lastly, the effect of PNIPAM chain length appeared to be less important on stabilization properties as less significant differences were observed when comparing polymer with the same hyperbranched core bearing P2, P5 or P7. It is to be noticed that in the case of H4P7 and H5P7 a strong tendency to aggregation was observed (more pronounced in the case of H5P7). This could be ascribed to some difficulties of this polymer of high molecular mass to interact efficiently with the NPs surface probably due to their specific conformation in solution. Therefore, these experiments tend to demonstrate in order to gain high colloidal stability that i) a branched structure is more efficient than the corresponding linear one, ii) an optimal size of the branched structures is required to be able to interact in an optimal way with the NPs surface. Largest structure obtained through the use of large core (H4 or H5) or of a longer PNIPAM chain will lead to less efficient stabilizing agent.

By assuming a perfect reduction of the gold salt and a NPs average diameter of 5 nm, the minimum density of adsorbed polymer to obtain good stabilization properties can be calculated from the minimal polymer concentration. Values obtained were in the range of $3 \cdot 10^4 \text{ ng} \cdot \text{cm}^{-2}$. These high values suggested that a large excess of polymer is needed to obtain good stabilization properties in the chosen conditions. Indeed, TEM images obtained after negative staining of dispersions of PNIPAM-coated AuNPs confirmed the formation of a thick layer of PNIPAM around NPs (see Figure S19 in ESI).²⁸ On TEM images, the hybrid Au/polymer particles clearly showed to have a core-shell morphology, the dark cores corresponding to the electron-dense Au atom embedded into a circular brighter polymer shell. The overall sizes of those composites were $8.5 \pm 2.6 \text{ nm}$. Numerous free polymer globules were also present in the case of copolymer coated NPs when polymer concentration was far beyond the capacity of AuNPs surfaces to interact with polymer.

In order to assess the effect of macromolecular architecture on the thermoresponsive properties, the changes in the surface plasmon band of AuNPs as a function of temperature was followed as shown in Figure 9. Indeed, the surface plasmon band of AuNPs was sensitive to many factors including the refractive index in the surroundings of the NPs. The influence of turbidity of the solution was removed by first subtracting the increase in absorbance at 400 nm and then by normalizing the curves in a way that these absorbances vary from 1 to 0.

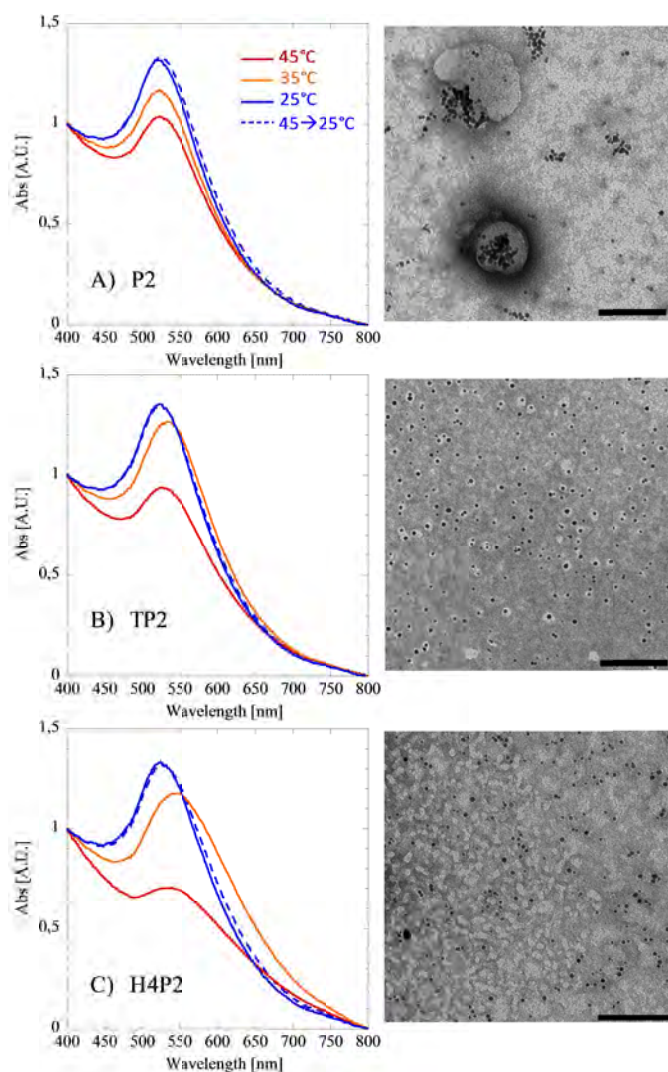


Figure 9. Changes in absorption spectra of Au@P2, Au@TP2 and Au@H4P2 with increasing temperature and corresponding TEM images of samples deposited at 45°C. The absorbance at 800 nm was subtracted from the spectra, then normalized at 400 nm to remove scattering contribution and multiplied by a factor in a way that absorbance vary from 0 to 1. [AuNPs]= $2.5 \cdot 10^{-4}$ mol·L⁻¹ and [polymer]=0.05 wt %.

Whereas, as expected no modification in absorption spectrum occurs for pristine gold NPs (i.e. in absence of thermoresponsive coating polymer, see Figure SI 20 in ESI), significant changes were observed for NPs coated with thermoresponsive polymers (Figure 9 and Figure SI21 in ESI). The collapse of PNIPAM at LCST due to the dehydration of the polymer chains usually induced a significant decrease of I_{\max} and a slight modification of λ_{\max} .⁷ Whereas this effect was clearly observed in the case of Au@P2 (Figure 9A), amplitude of those modifications increased significantly in the case of Au@TP2 and Au@H4P2 (Figures 9B and 9C). Such discrepancies could not belong to an aggregation phenomenon of nanohybrids induced by the increase of temperature: indeed TEM images obtained from sample deposited above T_c showed well dispersed individual NPs that does not differ significantly from the one observed below T_c

(see Figures S22-23 in ESI). In addition, these changes in the surface plasmon band were observed to be reversible as the temperature was lowered back to 25°C upon several heating-cooling cycles (Figure SI24 in ESI). Therefore, such differences may be mainly ascribed to the molecular architecture of the polymer in direct interaction with the surface of the NPs. Branched or hyperbranched structures allowed to obtain more densely packed inner layer around the NPs surface. This induces both higher sensitivity to dehydration phenomenon and higher efficiency as stabilizing agent of metallic NPs as demonstrated above.

To conclude, this first set of experiments based on the use of preformed NPs demonstrates that hyperbranched structures interact more efficiently with NPs than their linear counterpart and therefore act as better stabilizing agents. Nevertheless, higher colloidal stability is obtained with TREN based structures. This suggests higher efficiency of the latter to interact with the surface of gold NPs in a more densely packed layer.

In situ formation of AuNPs. The last and more striking evidence of the effects of molecular architecture was given by the controlled growth of particles in the presence of polymer (figure 10).

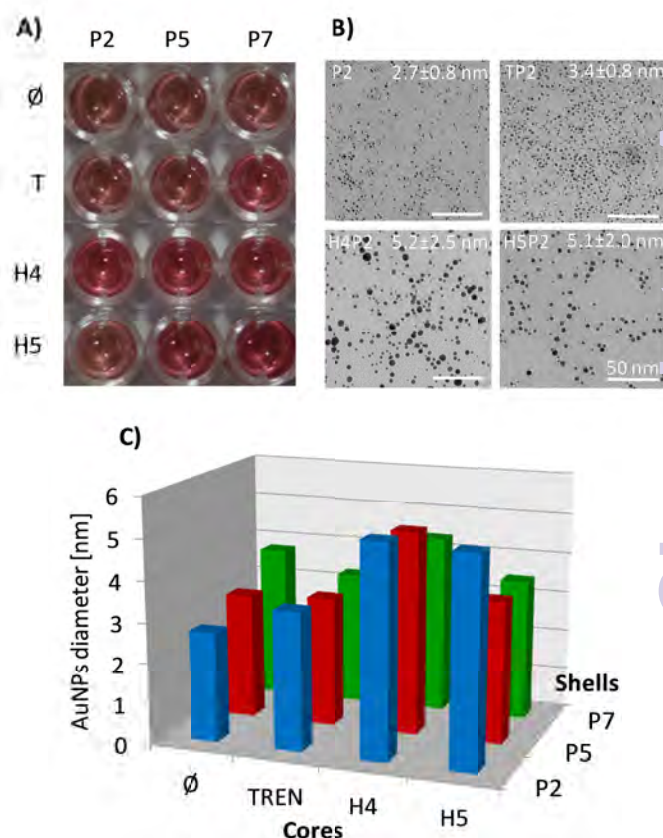


Figure 10. A) In situ synthesized AuNPs in HxPiY polymer aqueous solutions using NaBH₄ as reductant, [NaBH₄]/[Au] = 10, [Au] = 2.5×10^{-4} mol·L⁻¹, [polymer] = 0.01 wt. %. B) TEM images of in situ synthesized AuNPs. [AuNPs]= 2.5×10^{-4} mol·L⁻¹ and [polymer]=0.01 wt.%. Corresponding size histograms were given in figure SI25 in ESI). C) In situ synthesized AuNP sizes measured from TEM images. [AuNPs]= 2.5×10^{-4} mol·L⁻¹ and [polymer]=0.01 wt.%.

For those experiments, polymer concentrations of 0.01 wt % was chosen because an efficient stabilization is provided in such conditions. The formation of NPs was followed by UV-Vis measurements and transmission electron microscopy. After reduction, the final solution color, which is related to the surface plasmon band wavelength and was obtained in few minutes, varied from red to light orange depending on the polymer used (see Figure 10A). This clearly evidences the formation of gold nanoparticles of different size (see Figures SI28-30 in ESI). TEM images of the so-obtained hybrids NPs confirmed that the macromolecular structure had a strong influence on the final size and polydispersity of particles (see Figure 10 and Figures SI25-27 in ESI).

As described above in the absence of polymer, NPs with an average diameter of 5 ± 2 nm were obtained. Addition of polymer strongly modified this average size suggesting that they play a critical role on nucleation-growth process. In the case of linear PNIPAM, the mean size of particles was 2.7 ± 0.8 , 3.1 ± 0.8 and 3.8 ± 1.2 nm for P2, P5 and P7 respectively. Thus increasing macromolecules length tends to increase the average size of the obtained NPs. This difference in size can be correlated to different level of interaction during NPs growth mechanism. Small polymers seem to interact strongly with NPs surface as they can diffuse and rearrange more quickly onto these surface at the early stage of the NPs growth. Such interactions seems to be less efficient for larger polymers during the growing step as NPs presented size similar to the one of the control experiment (i.e. without stabilizing agent). This trend was confirmed when PNIPAM moiety was grafted on branched core. For a given PNIPAM chain length, increasing the size of the core, i.e. increasing the final macromolecular masses, induces an increase of gold NPs size: hence, in the case of P2, the size of NPs increase to 3.4 ± 0.8 , 5.2 ± 2.5 and 5.1 ± 2.0 nm respectively for TP2, H4P2 and H5P2. Similar trends were observed for other PNIPAM chain length.

Moreover, in the case of branched structures, a slower kinetics of formation of NPs is evidenced as slight changes of color occur with time within the first hours. This could be related to efficient interactions of those structures with gold ions that could slow down the growing mechanism. Nevertheless, as demonstrated in the previous part, hyperbranched act as better stabilizing agent than their linear counterparts once the colloidal solutions are obtained. Even if those large structures rearrange probably more slowly with NPs surface preventing them to be a good growth control agent, their specific structure allows them to hinder more efficiently the NPs surface and thus to avoid aggregation. TREN structures offered the best compromise to gain a control over NPs growth and to get colloidal solutions with high stabilization properties.

D. Conclusion

PNIPAM-based hyperbranched structures were prepared from different branched core using and their properties were studied in aqueous solutions. Those experiments permit to assess a strong relationship between macromolecular

architecture and thermoresponsiveness of those polymers. These polymers were then employed as stabilizers of AuNPs dispersions by either *a posteriori* adsorption on AuNPs or *in situ* formation. Both approaches were successful for stabilization and reversibility of the thermostimulable precipitation process was demonstrated. Moreover, we showed that, macromolecular architecture greatly influence growth mechanism of *in situ* formed NPs and the colloidal stability of the obtained nanohybrids. Whereas small linear polymers allowed a better control on NPs growth, branched structures proved to be better stabilizing agent. Moreover, for this purpose, TREN based structures were found to be more efficient than highly branched structures HYPAM. This strategy should be easily applied to other type of metallic NPs, and should lead to useful "smart" materials for a range of applications including drug-delivery devices and catalyst.

Acknowledgements

The authors acknowledge the EU for financial support on acquiring DSC apparatus (FEDER-35477).

Notes and references

Abbreviations. HYPAM: hyperbranched polyamidoamine, TREN: Tris(2-aminoethyl)amine, PNIPAM: poly(N isopropylacrylamide), Tc: cloud point temperature, LCST: lower critical solution temperature, NPs: nanoparticles, ATR-FTIR: attenuated total reflection- Fourier transform infrared red, PGSE NMR: pulsed gradient spin-echo nuclear magnetic resonance spectroscopy, DSC: Differential Scanning Calorimetry, TEM: transmission electron microscopy, SANS: small angle neutron scattering, DLS: Dynamic light scattering, SEC: size exclusion chromatography.

- 1 M. I. Gibson and R. K. O'Reilly, *Chem. Soc. Rev.*, 2013, **42**, 7204.
- 2 M. Beija, J.-D. Marty and M. Destarac, *Chem. Commun.*, 2011, **47**, 2826.
- 3 J. Liu, A. Debuigne, C. Detrembleur and C. Jérôme, *Adv. Health. Mater.*, 2014, **3** (12), 1941.
- 4 J.-F. Lutz, Ö. Akdemir and A. Hoth, *J. Am. Chem. Soc.*, 2006, **128**, 13046.
- 5 B. Verdonck, E. J. Goethals and F. E. Du Prez, *Macromol. Chem. Phys.*, 2003, **204**, 2090.
- 6 L. H. Gan, Y. Y. Gan and G. R. Doon, *Macromolecules*, 2000, **33**, 7893.
- 7 S. Sistach, M. Beija, V. Rahal, A. Brûlet, J.-D. Marty, M. Destarac and C. Mingotaud, *Chem. Mater.*, 2010, **22**, 3712.
- 8 Z.-P. Xiao, K.-M. Yang, H. Liang and J. Lu, *J. Polym. Sci. Part Polym. Chem.*, 2010, **48**, 542.
- 9 R. Plummer, D. J. T. Hill and A. K. Whittaker, *Macromolecules*, 2006, **39**, 8379.
- 10 A. K. A. S. Brun-Graepi, C. Richard, M. Bessodes, D. Scherman and O. W. Merten, *Prog. Polym. Sci.*, 2010, **35**, 1311.
- 11 Z. M. O. Rzaev, S. Dinçer and E. Pişkin, *Prog. Polym. Sci.*, 2007, **32**, 534.
- 12 M. Beija, J.-D. Marty and M. Destarac, *Prog. Polym. Sci.*, 2011, **36**, 845.
- 13 M. Beija, E. Palleau, S. Sistach, X. Zhao, L. Ressler, C. Mingotaud, M. Destarac and J.-D. Marty, *J. Mater. Chem.*, 2010, **20**, 9433.
- 14 J. Shan and H. Tenhu, *Chem. Commun.*, 2007, **43**, 4580.

- 15 Y. Shen, M. Kuang, Z. Shen, J. Nieberle, H. Duan and H. Frey, *Angew. Chem. Int. Ed.*, 2008, **47**, 2227.
- 16 X.-Y. Liu, F. Cheng, Y. Liu, H.-J. Liu and Y. Chen, *J. Mater. Chem.*, 2009, **20**, 360.
- 17 X.-Y. Liu, F. Cheng, Y. Liu, W.-G. Li, Y. Chen, H. Pan and H.-J. Liu, *J. Mater. Chem.*, 2009, **20**, 278.
- 18 N. Pérignon, J.-D. Marty, A.-F. Mingotaud, M. Dumont, I. Rico-Lattes and C. Mingotaud, *Macromolecules*, 2007, **40**, 3034.
- 19 C. Hajji and R. Haag in *Dendrimer Catalysis*; Gade, L. H., Ed.; Topics in Organometallic Chemistry; Springer Berlin Heidelberg, 2006; pp 149.
- 20 X. Hu, L. Zhou and C. Gao, *Colloid Polym. Sci.*, 2011, **289**, 1299.
- 21 A. Fahmi, D. Appelhans, N. Cheval, T. Pietsch, C. Bellmann, N. Gindy and B. Voit, *Adv. Mater.*, 2011, **23**, 3289.
- 22 F. Liu and M.W. Urban, *Prog. Polym. Sci.*, 2010, **35**, 3.
- 23 N. Pérignon, A.-F. Mingotaud, J.-D. Marty, I. Rico-Lattes and C. Mingotaud, *Chem. Mater.*, 2004, **16**, 4856.
- 24 S. Saliba, C. Valverde-Serrano, J. Keilitz, M. L. Kahn, C. Mingotaud, R. Haag and J.-D. Marty, *Chem. Mater.*, 2010, **22**, 6301.
- 25 R. M. Crooks, B. I. L. Lij, L. Sun, L. K. Yeung and M. Zhao in *Dendrimers III*; Vögtle, P. D. F., Ed.; Topics in Current Chemistry; Springer Berlin Heidelberg, 2001; pp 81.
- 26 H. H. Nguyen, C. Valverde Serrano, P. Lavedan, D. Goudouneche, A.-F. Mingotaud, N. Lauth-de Viguierie and J.-D. Marty, *Nanoscale*, 2014, **6**, 3599.
- 27 V. M. Garamus, T. V. Maksimova, H. Kautz, E. Barriau, H. Frey, U. Schlotterbeck, S. Mecking and W. Richtering, *Macromolecules*, 2004, **37**, 8394.
- 28 D. A. Tomalia, A. M. Naylor and W. A. Goddard, *Angew. Chem. Int. Ed. Engl.*, 1990, **29**, 138.
- 29 S. Nowag, C. Frangville, G. Multhaup, J.-D. Marty, C. Mingotaud and R. Haag, *J. Mater. Chem. B Mater. Biol. Med.*, 2014, **2**, 3915.
- 30 M. R. Radowski, A. Shukla, H. von Berlepsch, C. Böttcher, G. Pickaert, H. Rehage and R. Haag, *Angew. Chem. Int. Ed.*, 2007, **46**, 1265.
- 31 H. H. Nguyen, B. Payré, J. Fitremann, N. Lauth-de Viguierie and J.-D. Marty, *Langmuir*, 2015, **31**, 4761.
- 32 S. Sistach, K. Rahme, N. Pérignon, J.-D. Marty, N. Lauth-de Viguierie, F. Gauffre and C. Mingotaud, *Chem. Mater.*, 2008, **20**, 1221.
- 33 A. Glaria, M. Beija, R. Bordes, M. Destarac, and J.-D. Marty, *Chem. Mater.*, 2013, **25**, 1868.